Solid State Ionics 179 (2008) 2031-2036

Contents lists available at ScienceDirect

Solid State Ionics

journal homepage: www.elsevier.com/locate/ssi

Effect of effective areas on ionic conductivity in dense composite material composed of ionic and electronic conductors for solid oxide fuel cells

Changbo Lee, Joongmyeon Bae *

Department of Mechanical Engineering, Korea Advanced Institute of Science and Technology, 373-1 Guseong-Dong, Yuseong-Gu, Daejeon 305-701, Republic of Korea

ARTICLE INFO

Article history:
Received 5 February 2008
Received in revised form 21 June 2008
Accepted 23 June 2008

Keywords:
Ionic conductivity
Effective area
Oxygen reduction reaction
Composite material
Double-layered cathode

ABSTRACT

An ionic conductivity model for a dense composite material composed of an ionic conductor and an electronic conductor is investigated by considering effective areas. It was found that the effective areas of the oxygen reduction reaction at the material surface and the oxygen ion conduction through the material bulk are important factors for determining the ionic conductivity of the composites, although the oxygen reduction reaction per se is not a factor. The area-specific resistances (ASR) of single-layered and double-layered cathodes composed of $La_{0.8}Sr_{0.2}MnO_3$ (LSM-82) and $Zr_{0.85}Y_{0.15}O_2$ (YSZ) were measured and compared with the values predicted by the model. The degree of agreement between the measured and predicted ASR values validates the model for ionic conductivity in dense composite materials. Their impedance spectra were analyzed to support the results.

1. Introduction

$La_{1-x}Sr_xMnO_3$ (LSM) oxide is generally used as the cathode of solid oxide fuel cells (SOFCs). LSM cathodes have low levels of chemical reactivity and good thermal expansion compatibility with yttria-stabilized zirconia (YSZ). However, they have low ionic conductivity, which results in poor oxygen reduction reactions. Both the oxygen diffusivity and oxygen surface exchange kinetics of LSM oxides are low compared to those of cobalt-containing perovskite oxides [1–5]. Composite cathodes composed of LSM and YSZ have been investigated extensively with the intention of enhancing the coefficients of the oxygen diffusion and surface exchange [2,6–13]. LSM and YSZ are assumed to be a pure electronic conductor and a pure ionic conductor, respectively, at typical SOFC operational temperatures and pressure ranges. For this reason, the ionic conductivity of composite cathodes is typically estimated by taking into account the connectivity and ionic conductivity of the ionic conductor [6]. However, an oxygen reduction reaction must occur when measuring the ionic conductivity of a certain material (Fig. 1), which implies that it is one of the most important factors for oxygen mass transport in bulk material. If the oxygen reduction reaction is not generated at the material, measuring the ionic conductivity becomes impossible. Note that, however, the resistance of the oxygen reduction reaction itself is not a factor that directly determines the ionic conductivity in general because the ionic conductivity of material is measured usually by the 4-probe DC technique or the AC impedance technique with good electrodes to exclude the influence of oxygen reduction reaction. In other words, the ionic conductivity only indicates the level of ion conduction in bulk and it does not involve the oxygen reduction reaction at the surface. However, if the electrode property becomes worse, the ionic conductivity is gradually influenced by the effective area of the oxygen reduction reaction at the material surface, not the resistance of it. Such thinking must be increasingly correct in case of measuring the ionic conductivity of a composite material composed of an ionic conductor and an electronic conductor because the best pathway to reduce oxygen to oxygen ion at the surface is the triple phase boundary (TPB) with which the ionic conductor, the electronic conductor, and the oxygen gas are in contact, not the electrode, such as Pt. Therefore, both the effective areas participating in oxygen reduction reactions and oxygen ion conduction should be considered to predict the level of ionic conductivity of a composite material.

The primary objective of this paper is to formulate a simple model of the ionic conductivity of a dense composite material composed of an ionic conductor and an electronic conductor by reflecting on the aforementioned effective areas. The model is verified by comparing its calculated ionic conductivities with measured values from previous studies and by analyzing the area-specific resistance (ASR) properties and the impedance spectra of composite cathodes composed of $La_{0.8}Sr_{0.2}MnO_3$ (LSM-82) and $Zr_{0.85}Y_{0.15}O_2$ (YSZ) on YSZ electrolyte. Two types of cathode are used: a porous single-layered cathode and a double-layered cathode composed of a porous layer and a thin dense layer. The impedance of the LSCF double-

* Corresponding author. Tel.: +82 42 869 3045; fax: +82 42 869 8207.
E-mail addresses: leecb@kaist.ac.kr (C. Lee), jmbae@kaist.ac.kr (J. Bae).

0167-2738/$ – see front matter © 2008 Elsevier B.V. All rights reserved.
doi:10.1016/j.ssi.2008.06.018

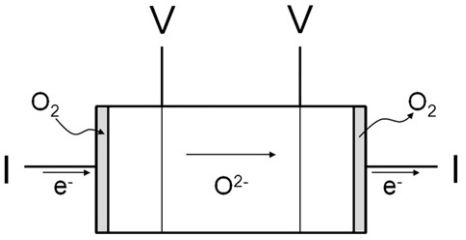

Fig. 1. Schematic of a general direct current method for measuring the ionic conductivity of a material.

layered cathode was found to be approximately 1 order of magnitude smaller than that of the single-layered cathode [14]. It follows that the LSM-82/YSZ double-layered cathode was prepared initially with the intention of decreasing the cathode impedance. From this point of view, the feasibility or limitation of the use of the double-layered cathode is investigated.

2. Experimental

LSM-82 was prepared using the glycine nitrate process (GNP) as described previously [15,16]. The resultant powder was calcined at 1000 °C for 1 h so that single crystal phases could be obtained. The composite cathode composed of LSM-82 and YSZ was prepared by mixing LSM-82 and YSZ at a weight ratio of 1:1 with 200 wt.% ethanol, ball-milling the slurry for 48 h, and finally drying it at 200 °C.

YSZ fine powder (Tosoh TZ-8Y) was used to prepare electrolyte pellets. The powders were pressed uniaxially in a circular mold at 2 MPa. The resulting green pellets were sintered at 1500 °C for 4 h in air, resulting in dense YSZ pellets that were approximately 26 mm in diameter and 2 mm thick. The pellets were cleaned with hydrofluoric acid for 1 min to remove any siliceous material, as SiO_2 in raw YSZ pellets can block the electrical conduction paths or reaction sites [14].

$La(NO_3)_3{\cdot}6H_2O$, $Sr(NO_3)_2$, $Mn(NO_3)_2{\cdot}4H_2O$, $ZrO(NO_3)_2{\cdot}xH_2O$ and $Y(NO_3)_3{\cdot}6H_2O$ were selected as the starting materials to create the sol of LSM-82/YSZ. The amounts of the nitrate hydrates for a 1:1 ratio of LSM-82 and YSZ in mole fractions were calculated and they were mixed with polyethylene glycol (PEG) of 2.5 mol% and deionized water of 1000 wt.% in a glass beaker. The mixed solution was stirred at 80 °C for 5 h to form the desired sol. The YSZ pellets were coated on both sides with the sol, and the organic matter of the coated sol was burned out by heating at 380 °C for 1 h. Coating with sol was repeated once more using the same procedure to produce the LSM-82/YSZ-layered YSZ pellets. The formation of the desired crystal phases (LSM-82 and YSZ) was checked by X-ray diffraction (XRD) analysis (Fig. 2). The patterns of YSZ and LSM-82 were measured using a powder X-ray diffractometer and the pattern of the LSM-82/YSZ thin dense layer was verified using a thin-film X-ray diffractometer. It was assumed that the phases of the LSM-82 and YSZ were formed independently and there were no chemical reactions between them. Therefore, it was expected that the TPB at the coated surface would increase due to the small size of the particles in the sol–gel-derived LSM-82/YSZ cathode.

The cathode powders were screen-printed in circles with a diameter of 10 mm on both sides of the YSZ or LSM-82/YSZ-layered YSZ pellets. The cathode was sintered at 1200 °C for 1 h in air, yielding a symmetrical half cell that was observed using a scanning electron microscope (SEM) (Fig. 3). It can be seen that the double-layered cathode was composed of a porous LSM-82/YSZ layer and a thin dense LSM-82/YSZ layer with a thickness of approximately 0.5 μm. The particles in the thin dense layer were approximately 10 times smaller than in the porous layer.

The impedances of the cathodes were measured in the open circuit voltage (OCV) state with a sweep voltage of 50 mV from 10^6 Hz to 10^{-2} Hz. The experimental temperature ranged from 500 °C to 900 °C in air. The ASR values of the cathode, in units of Ω cm^2, were calculated by taking into account the half cell symmetry (Eq. (1)):

$$\mathrm{ASR} = \frac{R_c}{2} \cdot A_c \tag{1}$$

where R_c and A_c represent the resistance and area of the cathode, respectively.

3. Model

Four assumptions were made for the model representing the ionic conductivity of a dense composite material, as follows:

(1) An oxygen reduction reaction of dense composite material at the grain boundary, which implies the boundary of ionic–electronic conductors, ionic–ionic conductors, or electronic–electronic conductors, is much more active than that at the grain surface, which implies the surface of an ionic conductor or an electronic conductor (Fig. 4). There is evidence to support this assumption. The oxygen surface exchange coefficient for LSM/YSZ composites was found to be approximately 1 to 2 orders of magnitude greater than that of LSM or YSZ single phase, even though the oxygen diffusion coefficient for LSM/YSZ is lower than that of YSZ [2]. Provided that the oxygen surface exchange reaction at the grain surface is more active than that at the grain boundary, the oxygen surface exchange coefficient for LSM/YSZ should be equivalent to or lower than that of LSM or YSZ because the total surface area is unchanged. This is the reverse of the actual phenomenon, assuming that the assumption is feasible.
(2) The grains of the ionic conductor and electronic conductor are hexagonal and are the same size at the material surface (Fig. 4). This is because the composite material is fabricated usually by sintering.
(3) The longitudinal resistivity of the ionic conduction is much greater than the lateral resistivity. The longitudinal direction is perpendicular to the direction of the material surface.
(4) The ions in the ionic conductor and electronic conductor are conducted individually through the same material and not transferred from the ionic conductor to the electronic conductor, and vice versa.

Let the volumetric fraction of the ionic conductor be α. Now consider the ionic conduction in the network of the ionic conductor. Each effective area caused by an oxygen reduction reaction at the material surface and by oxygen ionic conduction at the material bulk should be determined because the ionic conductivity is governed by these factors,

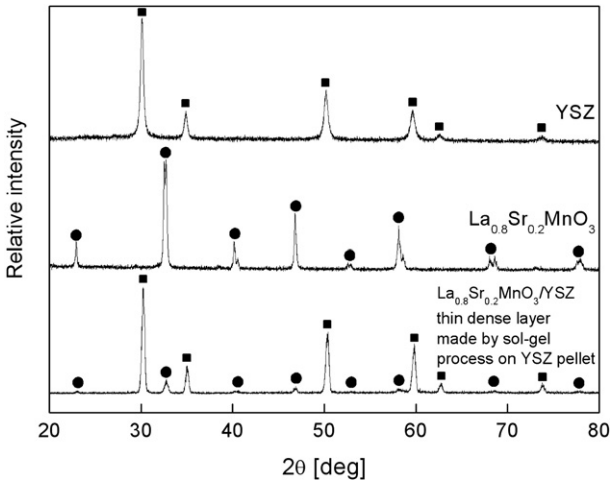

Fig. 2. XRD patterns of YSZ (■), LSM-82 (●) and LSM-82/YSZ thin dense layers on YSZ pellets.

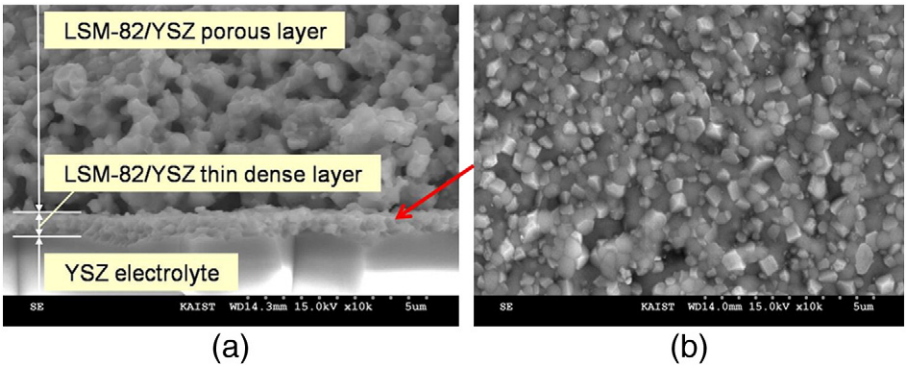

Fig. 3. SEM images of a LSM-82/YSZ double-layered half cell sintered at 1200 °C for 1 h. (a) Cross-section. (b) Surface of a thin dense layer.

as explained in the introduction of this paper. This section begins by considering the effective area of the oxygen reduction reaction. It is known that the TPB with which LSM, YSZ, and the oxygen gas are in contact is the most favorable pathway for oxygen reduction reactions [2,17]. The fraction of the TPB (pair of ionic–electronic conductors) compared to all boundaries (pairs of ionic–electronic conductors, ionic–ionic conductors, and electronic–electronic conductors) can be calculated from Fig. 4 by the probability theory, as follows:

$$\frac{\text{Number of ionic}-\text{electronic conductor boundary}}{\text{Number of all boundaries}} = 2\alpha(1-\alpha) \tag{2}$$

Therefore, the effective area for the oxygen reduction reaction in terms of the ionic conductor ($A^{i}_{\text{eff},k}$) must be defined as follows:

$$A^{i}_{\text{eff},k} = 2\alpha(1-\alpha)\cdot A_m \quad \left(\alpha < \alpha^{i}_{c}\right) \tag{3}$$

where A_m and α^{i}_{c} denote the measuring area of the electrical property and the critical fraction in terms of the ionic conductor, respectively. $A^{i}_{\text{eff},k}$ increases initially as α increases, but $A^{i}_{\text{eff},k}$ decreases conversely as α increases past the turning point at α=0.5, according to Eq. (3). However, if the fraction of the ionic conductor is greater than the critical fraction ($\alpha > \alpha^{i}_{c}$), the effective area of the oxygen reduction reaction will increase as the fraction of the ionic conductor increases because the grain boundaries of the ionic–ionic conductors become active. Hence, the effective area for the oxygen reduction reaction should be recalculated by taking into account the fraction of the pairs of ionic–ionic conductors if $\alpha > \alpha^{i}_{c}$.

$$\frac{\text{Number of ionic}-\text{ionic conductor boundary}}{\text{Number of all boundaries}} = \alpha^2 \tag{4}$$

$$A^{i}_{\text{eff},k} = \alpha^2 \cdot A_m \quad \left(\alpha > \alpha^{i}_{c}\right) \tag{5}$$

Here, Eqs. (3) and (5) are valid when $\alpha<\alpha^{i}_{c}$ and $\alpha>\alpha^{i}_{c}$, respectively. It remains to discuss α^{i}_{c}. The critical fraction α^{i}_{c} can be determined when the exchanged oxygen flux at the pair of ionic–electronic conductors is equal to the flux at the pair of ionic–ionic conductors, as follows:

$$k_{i-i}A^{i}_{\text{eff},k}\left(\alpha > \alpha^{i}_{c}\right) = k_{i-e}A^{i}_{\text{eff},k}\left(\alpha < \alpha^{i}_{c}\right) \tag{6}$$

where k_{i-i} and k_{i-e} represent the oxygen reduction reaction coefficients of the pair of ionic–ionic conductors and of the pair of ionic–electronic conductors, respectively. Eq. (6) can be rearranged to obtain α^{i}_{c}, as follows:

$$\frac{k_{i-e}}{k_{i-i}} = \frac{\alpha^{i^2}_{c}}{2\alpha^{i}_{c}\left(1-\alpha^{i}_{c}\right)} \tag{7}$$

k_{i-e} is generally greater than k_{i-i} because the circumstances for ionization at the pair of the ionic–electronic conductors are superior to those at the counterpart. The values of α^{i}_{c} are 0.67, 0.95, and 0.99 when the values of k_{i-e}/k_{i-i} are 1, 10, and 100, respectively, according to Eq. (7). Now consider the effective area caused by oxygen ionic conduction in the composite material bulk. The effective area for ionic conduction in the ionic conductor ($A^{i}_{\text{eff},D}$) should be calculated with respect to the fraction and connectivity. The longitudinal resistivity was assumed to be much greater than the lateral resistivity in this study. Hence, the probability of contact between the former ionic conductor grain and the subsequent ionic conductor grain can be estimated as α^2 by simply multiplying the fractions of the ionic conductors. This yields the effective area of the ionic conduction in the ionic conductor, as follows:

$$A^{i}_{\text{eff},D} = \alpha^2 \cdot A_m \tag{8}$$

Therefore, the total effective area of the ionic conductor (A^{i}_{eff}) can be calculated by multiplying the effective areas for the oxygen reduction reaction (Eqs. (3) or (5)) and the ionic conduction (Eq. (8)).

$$A^{i}_{\text{eff}} = 2\alpha^3(1-\alpha)\cdot A_m \quad \left(\alpha < \alpha^{i}_{c}\right) \tag{9}$$

$$A^{i}_{\text{eff}} = \alpha^4 \cdot A_m \quad \left(\alpha > \alpha^{i}_{c}\right) \tag{10}$$

This section now analyses the ionic conduction in the electronic conductor. There is a clear similarity between the ionic conductivity of the ionic conductor and that of the electronic conductor. The total effective area of the electronic conductor ($A^{e}_{\text{eff},}$) can be arranged by

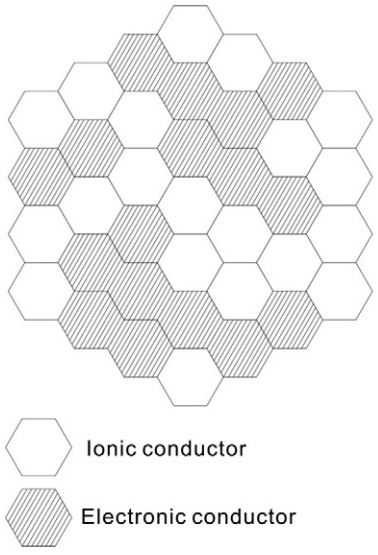

Fig. 4. Model surface composed of an ionic conductor and an electronic conductor.

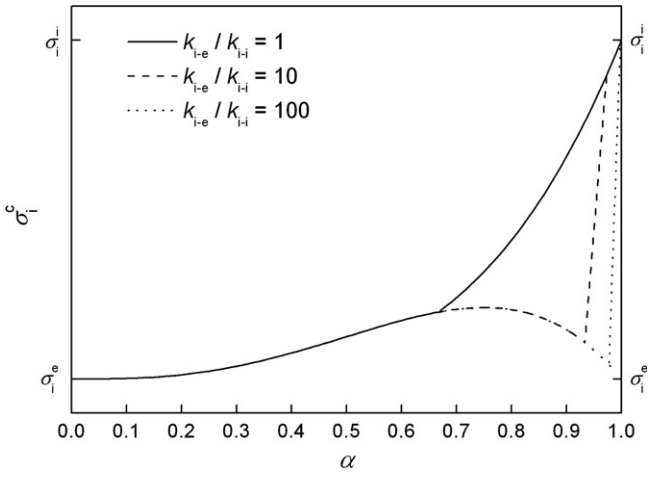

Fig. 5. Model ionic conductivity of a composite electrode composed of an ionic conductor and an electronic conductor as a function of the ionic conductor fraction and oxygen surface exchange kinetics (The curves are described in decimal scale when σ_i^i is 4 orders of magnitude greater than σ_i^e).

applying the aforementioned formulations evenly to the electronic conductor.

$$A_{eff}^e = 2\alpha(1-\alpha)^3 \cdot A_m \quad (\alpha > \alpha_c^e) \tag{11}$$

$$A_{eff}^e = (1-\alpha)^4 \cdot A_m \quad (\alpha < \alpha_c^e) \tag{12}$$

where α_c^e denotes the critical fraction in terms of the electronic conductor. α_c^e can also be determined by comparing the oxygen fluxes at the pairs of ionic–electronic conductors and electronic–electronic conductors.

$$\frac{k_{i-e}}{k_{e-e}} = \frac{(1-\alpha_c^e)^2}{2\alpha_c^e(1-\alpha_c^e)} \tag{13}$$

where k_{e-e} represents the oxygen reduction reaction coefficient for the pair of electronic–electronic conductors. α_c^e is estimated to be 0.33, 0.05, and 0.01 when the values of k_{i-e}/k_{e-e} are 1, 10, and 100, respectively,

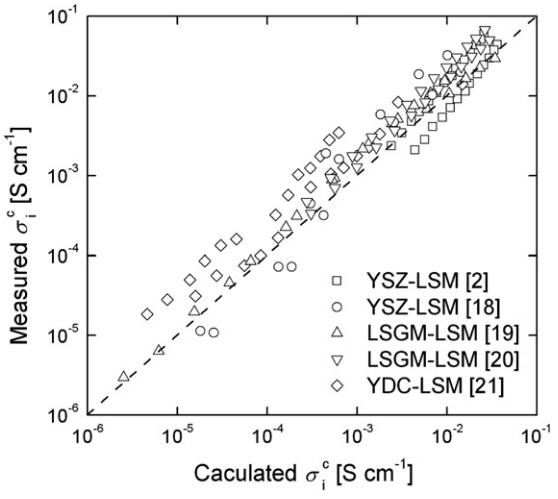

Fig. 6. Comparisons of the calculated and measured ionic conductivities of several composites (□: $Zr_{0.85}Y_{0.15}O_2$–$La_{0.8}Sr_{0.2}MnO_3$ [2], ○: $Zr_{0.85}Y_{0.15}O_2$–$La_{0.65}Sr_{0.3}MnO_3$ [18], △: $La_{0.83}Sr_{0.17}Ga_{0.83}Mg_{0.17}O_{2.83}$–$La_{0.8}Sr_{0.2}MnO_3$ [19], ▽: $La_{0.9}Sr_{0.1}Ga_{0.8}Mg_{0.2}O_3$–$La_{0.9}Sr_{0.1}MnO_3$ [20], ◇: $Ce_{0.8}Y_{0.2}O_2$–$La_{0.7}Sr_{0.3}MnO_3$ [21]; the data showing the ionic conduction behavior were selected from the electrical conductivity data in previous studies).

according to Eq. (13). The ionic conductivity for the composite material can be calculated by considering the effective areas.

$$\sigma_i^c = \frac{A_{eff}^i}{A_m} \cdot \sigma_i^i + \frac{A_{eff}^e}{A_m} \cdot \sigma_i^e \tag{14}$$

In Eq. (14), σ_i^c, σ_i^i, and σ_i^e denote the ionic conductivities of the composite material, the ionic conductor, and the electronic conductor, respectively. Eq. (14) can be reduced for practical situations in which $k_{i-e} \gg k_{i-i}$, $k_{i-e} \gg k_{e-e}$, and $\sigma_i^i \gg \sigma_i^e$, as follows:

$$\sigma_i^c = 2\alpha^3(1-\alpha) \cdot \sigma_i^i \tag{15}$$

Therefore, the ionic conductivity of the composite material can be expressed in terms of the fraction of the ionic conductor and in terms of the oxygen reduction reaction kinetics (Fig. 5). In order to validate the model, the calculated and measured ionic conductivities were compared (Fig. 6). Data for the comparison consisted of results of previous studies concerning the electrical conductivities of various types of ionic conductors and the composite materials that function as ionic conductors for various compositions at various temperatures [2,18–21]. It was considered feasible that both the effective areas of the oxygen reduction reaction at the composite material surface and the oxygen ionic conduction in the material bulk are important factors for determining the ionic conductivity.

4. Results and discussion

4.1. ASR properties

The ASR of the cathodes showed thermally activated behavior (Fig. 7). The activation energies of the single-layered LSM-82/YSZ composite cathode and double-layered LSM-82/YSZ composite cathode on YSZ were 1.63 and 1.33 eV, respectively. The activation energy of the double-layered cathode was lower than that of the single-layered cathode by 0.3 eV. The ASR was decreased by introducing the double-layered cathode at temperatures of 800 °C and below. The ASR of the double-layered cathode was measured as 0.52 Ω cm^2. This is lower than the single-layered cathode at 1.35 Ω cm^2 at a temperature of 700 °C.

4.2. Model validation by comparing ASR values

The particles in the thin dense layer were nearly 10 times smaller compared to those in the porous layer, as seen in Fig. 3. Due to this

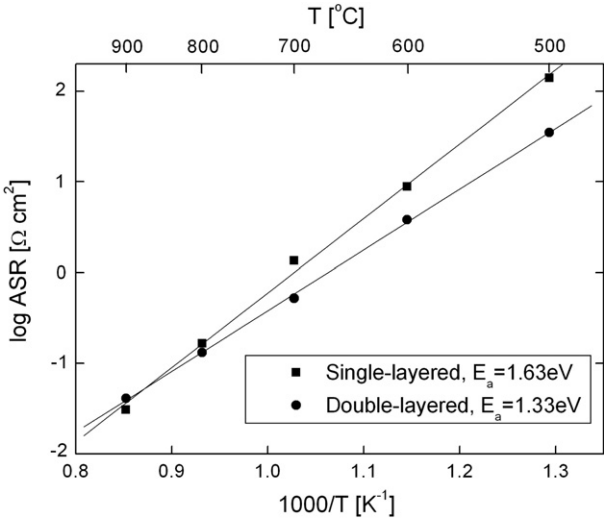

Fig. 7. Temperature dependence of ASR for single-layered and double-layered cathodes of LSM-82/YSZ on YSZ electrolyte.

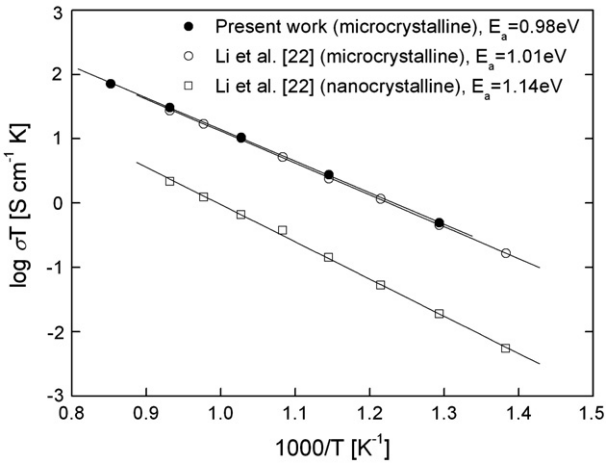

Fig. 8. Temperature dependence of the electrical conductivities of YSZ (microcrystalline vs. nanocrystalline).

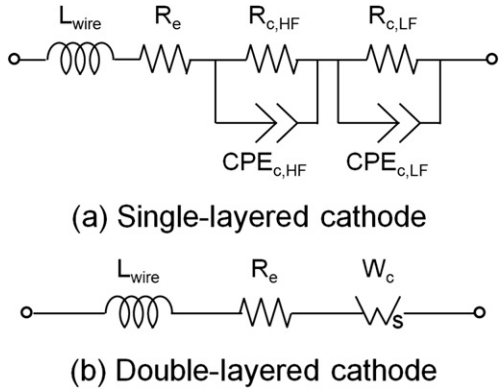

Fig. 10. Impedance models for (a) single-layered and (b) double-layered cathodes.

property of the thin dense layer, the length of the TPB layer was increased by approximately 100 times compared to that of the porous layer. Moreover, if the porosity of the cathode is also considered, the estimated TPB length is longer than that. As a result, the oxygen reduction reaction kinetics was improved substantially. However, the impedance of the double-layered cathode was 2–3 times smaller than that of the single-layered cathode in only the low temperature region, not 100 times smaller. This is because the oxygen ions should pass through the thin dense layer by bulk diffusion due to the lack of gas permeability. Therefore, the impedance depends strongly on oxygen ion diffusion in the thin dense layer. If the cathodic and anodic activations have symmetry, the ASRs of the single-layered cathode (ASR_s) and double-layered cathode (ASR_d) at OCV can be expressed as follows:

$$ASR_s = \frac{RT}{2Fi_{0,s}} \tag{16}$$

$$ASR_d = \frac{RT}{2Fi_{0,d}} = \frac{RT}{2Fi_{0,t}} + \frac{l}{\sigma_i} \tag{17}$$

where $i_{0,s}$ $i_{0,d}$, and $i_{0,t}$ denote the exchange current densities of the single-layered cathode, the double-layered cathode, and the thin dense layer, respectively. In addition, l and σ_i denote the thickness and ionic conductivity of the thin dense layer, respectively. R, T, and F have their standard meaning. The ASR_d can be rearranged using the relationship of $i_{0,s}$ and $i_{0,t}$. The ratio of $i_{0,t}/i_{0,s}$ was estimated to be approximately 100 in this study. σ_i can be calculated by the proposed model. The ionic conductivity for YSZ estimated from the half cell test result is in good agreement with that of the microcrystalline YSZ [22]. However, it is clear that the ionic conductivities for the microcrystalline and nanocrystalline YSZs are different due to the difference in the transferring number between grain boundaries. In this case, the ionic conductivity data for the nanocrystalline YSZ [22] (Fig. 8) were used because the sol–gel-derived thin dense layer was in nanoscale (~100 nm). The measured ASRs were compared with the predicted values calculated by Eq. (17) (Fig. 9). It was observed that the calculated data were in agreement with the measured data in terms of the ASR value, whereas a difference was noted at activation energies of approximately 0.3 eV. The activation energy of the calculated data naturally may follow that of the oxygen ion diffusion in YSZ because the rate-determining step is the oxygen ion diffusion in the thin dense layer. Contrary to this expectation, it was found that the activation energy of the oxygen diffusion in LSM-82/YSZ composites is approximately 1.3–1.4 eV in previous study [2], which is higher than that of pure YSZ. This fact may support the difference between the predicted and measured activation energies of the cathode. The prediction by the proposed model is fairly well established from the comparison of ASRs.

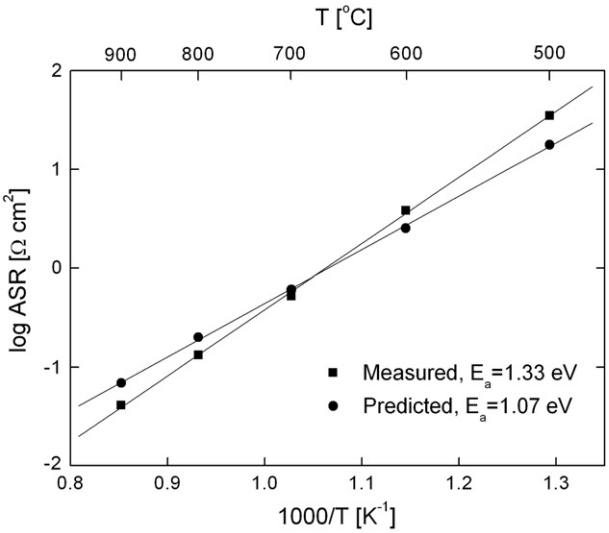

Fig. 9. Comparison of the measured and predicted ASRs with respect to temperature.

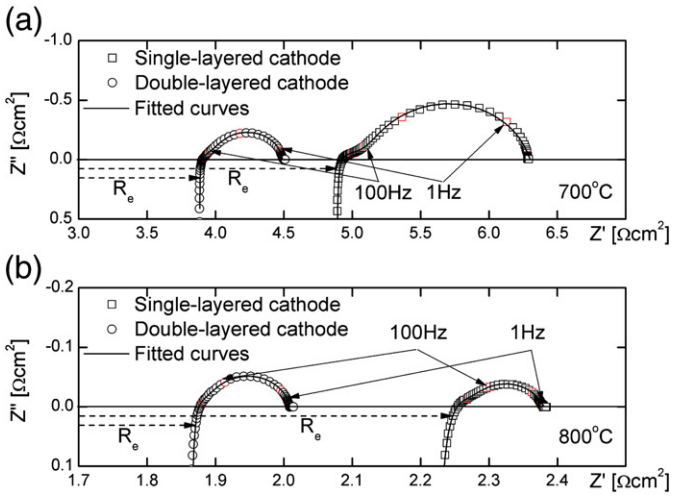

Fig. 11. Impedance spectra for single-layered and double-layered cathodes at (a) 700 °C and (b) 800 °C.

4.3. Model validation by comparing impedance spectra

The impedance spectra of the single-layered cathode and double-layered cathode were analyzed to support the rate-determining step of the cathodes (Figs. 10 and 11). The impedance of a typical single-layered LSM/YSZ composite cathode can be modeled as a series circuit including parallel combinations composed of the resistance (R) and the constant phase element (CPE) (Fig. 10(a)) [13,23,24]. The parallel circuit, $R_{c,HF}CPE_{c,HF}$, that appears as a semi-circle at the higher frequency region is attributed to the charge transfer from electrode to electrolyte, and the circuit of $R_{c,LF}CPE_{c,LF}$ at the lower frequency region is attributed to the oxygen reduction reaction that consists of gas diffusion, adsorption, dissociation, and surface/bulk diffusion [15,23,25]. One of the oxygen reduction reaction processes can be determined to be the rate-determining process by observing the oxygen partial pressure dependence [15]. The impedance of the double-layered cathode can be modeled using the Warburg element (Fig. 10(b)) [25,26]. This is because the rate-determining step was predicted, through ASR analysis, to be the oxygen ion diffusion in the thin dense layer rather than an oxygen reduction reaction at the porous layer or on the surface of the thin dense layer. The impedance spectra obtained by the experiments were fitted to the modeled spectra (Fig. 11). It follows from what has been explained that the proposed model for the ionic conductivity of a composite material is validated and sufficient for use in practical situations of SOFCs.

5. Conclusions

The ionic conductivity of a composite material composed of an ionic conductor and an electronic conductor was modeled by considering the effective areas derived by oxygen reduction reaction and oxygen ion conduction. The ionic conductivity generally increases as the fraction of the ionic conductor increases; however, the ionic conductivity can decrease conversely as the fraction increases in accordance with the critical fractions. In order to validate the model, the data predicted by the model were compared with measured data from previous studies. The differences between the predicted and measured data were in the range of half an order of magnitude, which is within acceptable boundaries. A comparison of the ASR and impedance spectra between single-layered and double-layered cathodes composed of LSM-82 and YSZ was carried out to support the model for ionic conductivity. The measured ASR values and impedance spectra were in good agreement with the predicted values and the modeled impedance spectra, respectively. This agreement confirms that the proposed model is useful for the experimental ranges.

Acknowledgements

This work is an outcome of the projects of the Best Lab program and the development program of Core Technologies for Fuel Cell (CTFC) by the Ministry of Knowledge Economy (MKE), and the Brain Korea 21 (BK21) program by the Ministry of Education, Science and Technology (MEST). The authors greatly appreciate their financial support.

References

[1] B.C.H. Steele, Solid State Ionics 86–88 (1996) 1223.
[2] Y. Ji, J.A. Kilner, M.F. Caloran, Solid State Ionics 176 (2005) 937.
[3] A.V. Berenov, J.L. MacManus-Driscoll, J.A. Kilner, Solid State Ionics 122 (1999) 41.
[4] R.A. De Souza, J.A. Kilner, Solid State Ionics 106 (1998) 175.
[5] R.A. De Souza, J.A. Kilner, Solid State Ionics 126 (1999) 153.
[6] K. Yamahara, T.Z. Sholklapper, C.P. Jacobson, S.J. Visco, L.C. De Jonghe, Solid State Ionics 176 (2005) 1359.
[7] A. Barbucci, M. Viviani, P. Carpanese, D. Vladikova, Z. Stoynov, Electrochimica Acta 51 (8–9) (2006) 1641.
[8] A. Barbucci, P. Carpanese, G. Cerisola, M. Viviani, Solid State Ionics 176 (2005) 1753.
[9] A. Barbucci, R. Bozzo, G. Cerisola, P. Costamagna, Electrochimica Acta 47 (13–14) (2002) 2183.
[10] M.J. Jørgensen, M. Mogensen, Journal of the Electrochemical Society 148 (5) (2001) A433.
[11] M.J. Jørgensen, S. Primdahl, M. Mogensen, Electrochimica Acta 44 (24) (1999) 4195.
[12] Y.J. Leng, S.H. Chan, K.A. Khor, S.P. Jiang, Journal of Applied Electrochemistry 34 (4) (2004) 409.
[13] T. Suzuki, M. Awano, P. Jasinski, V. Petrovsky, H.U. Anderson, Solid State Ionics 177 (2006) 2071.
[14] J.-M. Bae, B.C.H. Steele, Solid State Ionics 106 (1998) 247.
[15] C. Lee, S.-W. Baek, J. Bae, Solid State Ionics 179 (2008) 1465.
[16] C. Lee, J. Bae, Journal of Power Sources 176 (2008) 62.
[17] T. Horita, K. Yamaji, N. Sakai, H. Yokokawa, T. Kawada, T. Kato, Solid State Ionics 127 (2000) 55.
[18] C.-C.T. Yang, W.-C.J. Wei, A. Roosen, Materials Chemistry and Physics 81 (2003) 134.
[19] G. Dotelli, C.M. Mari, R. Ruffo, R. Pelosato, I. Natali Sora, Solid State Ionics 177 (2006) 1991.
[20] J.Y. Yi, G.M. Choi, Solid State Ionics 148 (2002) 557.
[21] G.S. Godoi, D.P.F. de Souza, Material Science and Engineering B 140 (2007) 90.
[22] Q. Li, T. Xia, X.D. Liu, X.F. Ma, J. Meng, X.Q. Cao, Material Science and Engineering B 138 (2007) 78.
[23] J.-D. Kim, G.-D. Kim, J.-W. Moon, Y.-I. Park, H.-W. Lee, K. Kobayashi, M. Nagai, C.-E. Kim, Solid State Ionics 143 (2001) 379.
[24] J.H. Choi, J.H. Jang, S.M. Oh, Electrochimica Acta 46 (2001) 867.
[25] Y.-M. Kim, S.-I. Pyun, J.-S. Kim, G.-J. Lee, Journal of the Electrochemical Society 154 (8) (2007) B802.
[26] A. Ringuedé, J. Fouletier, Solid State Ionics 139 (2001) 167.